Structural, Optical, Electrical and Morphological Study of Transparent p-NiO/n-ZnO Heterojunctions Grown by PLD

V. E. Sandana[(a)] , D. J. Rogers[(a)] , F. Hosseini Teherani[(a)], P. Bove[(a)], N. Ben Sedrine[(b)], M. R. Correia[(b)], T. Monteiro[(b)], R. McClintock[(c)] and M. Razeghi[(c)]

[(a)]Nanovation, 8 route de Chevreuse, Châteaufort, 78117, France.
[(b)]Departamento de Física & I3N, Universidade de Aveiro, Campus Universitário de Santiago, 3810-193 Aveiro, Portugal.
[(c)]Center for Quantum Devices, ECE Department, Northwestern University, Evanston, Illinois 60208, USA.

ABSTRACT

NiO/ZnO heterostructures were fabricated on FTO/glass and bulk hydrothermal ZnO substrates by pulsed laser deposition. X-Ray diffraction and Room Temperature (RT) Raman studies were consistent with the formation of (0002) oriented wurtzite ZnO and (111) oriented fcc NiO. RT optical transmission studies revealed bandgap energy values of ~3.70 eV and ~3.30 eV for NiO and ZnO, respectively and more than 80% transmission for the whole ZnO/NiO/FTO/glass stack over the majority of the visible spectrum. Lateral p-n heterojunction mesas (~6mm x 6mm) were fabricated using a shadow mask during PLD growth. n-n and p-p measurements showed that Ti/Au contacting gave an Ohmic reponse for the NiO, ZnO and FTO. Both heterojunctions had rectifying I/V characteristics. The junction on FTO/glass gave forward bias currents (243mA at +10V) that were over 5 orders of magnitude higher than those for the junction formed on bulk ZnO. At ~ 10^{-7} A (for 10V of reverse bias) the heterojunction leakage current was approximately two orders of magnitude lower on the bulk ZnO substrate than on FTO. Overall, the lateral p-NiO/n-ZnO/FTO/glass device proved far superior to that formed by growing p-NiO directly on the bulk n-ZnO substrate and gave a combination of electrical performance and visible wavelength transparency that could predispose it for use in various third generation transparent electronics applications.

Keywords: NiO, ZnO, transparent heterojunction, FTO, Glass, Pulsed Laser Deposition, p-type TCO

1. INTRODUCTION

Over the past decade there has been a surge in interest for transparent electronics because of a number of advances in materials and device engineering. These developments can be viewed as comprising three distinct generations [1]. The first generation consists of a number of well-established passive applications based on exploiting the combination of transparency and conductivity which is observed for a limited number of (mostly oxide) materials (e.g. window defrosting, filtering of ultraviolet and/or infrared light, electromagnetic shielding, transparent wiring, touch-sensitive panels, and transparent contacts for use in flat panel displays, solar cells, and light-emitting diodes (LEDs) etc.) [2]. The second transparent electronics generation involves active devices relying on the n-type semiconductor nature of some Transparent Conducting Oxide (TCOs) (usually amorphous zinc oxide (ZnO)-based alloys for the replacement of the amorphous silicon currently employed as the n-channel in transparent thin film transistors for active matrix liquid crystal displays, organic LED displays and systems on glass) [3]. The third generation of transparent electronics concerns the move on to bipolar and complementary p-n junction-based devices. Such devices are projected to form the building blocks of transparent integrated circuits and completely transparent electronic products with innovative new functionalities such as transparent displays or intelligent surfaces [3]. The emergence of this generation is currently being hampered by the lack of a suitable transparent p-type material with sufficient carrier concentration, conductivity and mobility for use in p-n junctions.

Oxide-based Materials and Devices VI, edited by Ferechteh H. Teherani, David C. Look, David J. Rogers,
Proc. of SPIE Vol. 9364, 93641O · © 2015 SPIE · CCC code: 0277-786X/15/$18 · doi: 10.1117/12.2177427

Face centred cubic (fcc) nickel oxide (NiO) was one of the first reported p-type TCOs [4]. It is a direct [5] wide bandgap (reported Eg between 3.4 & 4.3 eV) [6-8] semiconductor material with excellent electrochemical stability, an elevated conduction band energy level and a relatively high ionization potential. While stoichiometric NiO is electrically insulating, as-grown NiO is invariably reported to be Ni deficient [9] and shows p-type conduction with a hole concentration that increases with oxygen content. This is attributed to positive charge compensation (formation of two Ni^{3+} ions in order to maintain charge neutrality) at thermodynamically-favored Ni^{2+} vacancies [10, 11]. As a result of the inherent p-type nature, NiO has been investigated for wide range of existing and emerging applications [12]. It is extremely difficult to obtain in n-type form, however. Thus it is interesting to consider the possibility of creating a heterojunction with an alternative n-type transparent conductor.
Wurtzite (hcp) ZnO is also a direct wide bandgap material (Eg ~ 3.4 eV) with intrinsically high transparency over the whole visible range. Degenerately-doped wurtzite ZnO is currently displacing ITO for many first generation transparent conductor applications due to recent improvements in attainable conductivity combined with processing, cost and toxicity advantages [13]. In parallel, the past decade has seen the emergence of ZnO-based amorphous oxides for use in transparent thin film transistors which offer significant increases in the mobilities and Id on/off ratios compared to the amorphous-silicon-based select FETs currently used in AM-OLED and LCD screens [3]. With regards to p-n junction-based third generation transparent electronics, ZnO has the opposite problem from NiO in that, although there have been many reports of p-type doping in ZnO, it has proven difficult to obtain reliable/stable p-type doping with sufficient acceptor concentration and mobility/conductivity for most practical applications [14]. A number of contributory reasons are typically evoked for this including strong donor self-compensation produced by the interplay of hydrogen and other impurities with native defects (oxygen vacancies and zinc interstitials), which renders ZnO n-type, since non-intentionally-doped ZnO is invariably oxygen deficient.

There have already been a number of papers concerning the marrying of n-type ZnO with p-type NiO, particularly for LED [15,16] and photodetector [17, 18] applications. Recently, it has been suggested that the adoption of such junctions might be extended to other third generation transparent electronics applications [19, 20]. In this paper, we compare the properties of p-NiO/n-ZnO heterojunctions grown on commercial bulk hydrothermal ZnO and FTO/glass substrates by Pulsed Laser Deposition (PLD) with a view to such utilisation.

2. EXPERIMENT

2.1 NiO/ZnO heterostructure obtained using a bulk hydrothermal ZnO substrate

NiO layers were deposited directly onto the Zn-polar face of single-side-polished (Crystec) bulk hydrothermal ZnO substrates by PLD, using conditions described elsewhere [12]. This strategy was employed because hydrothermally-grown bulk ZnO contains lithium [21], which is known to be a good dopant for boosting the conductivity of NiO. Since it is a fast diffuser and mobile at 400°C it was hoped that this configuration might improve the device characteristics. A schematic representation of the structure is shown in Fig. 1 below:

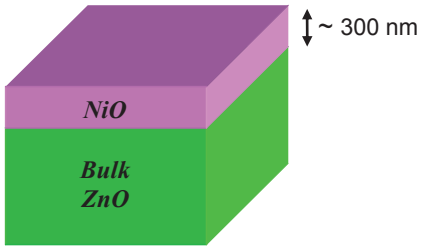

Figure 1 Schematic of the NiO/bulk ZnO structure

2.2 NiO/ZnO heterostructure grown on FTO/glass

ZnO and NiO layers were deposited using PLD with a pulsed KrF excimer laser (248nm) onto a glass substrate coated with degenerate Fluorine Tin Oxide (FTO) (provided by Solaronix) using the same conditions as those employed for the

NiO growth on the bulk ZnO substrates (above). Figure 2 shows a schematic of the heterostructure (with nominal film thicknesses indicated).

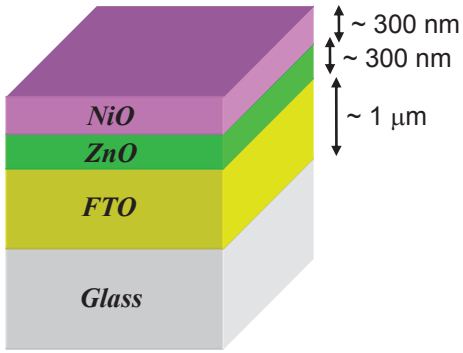

Figure 2 Schematic of the NiO/ZnO/FTO/glass heterostructure

Substrate temperature during deposition was limited to 400°C because of the temperature-sensitivity of the FTO/glass.

2.3 Characterisation

X-ray diffraction (XRD) studies were conducted with a Panalytical MRD high resolution diffractometer system. A Philips XL-30 Field Emission Gun-Scanning Electron Microscopy (FEG-SEM) was used to examine the film thickness and surface morphology. Electrical transport measurements were made with a Keithley 2400 source-meter, a Signatone four-collinear-probe resisitivity measurement system and a Karl Suss probe station. Room Temperature (RT) optical transmission studies were performed using an Ocean Optics system comprising a halogen lamp, a deuterium lamp and a Maya spectrometer. RT Raman studies were made in a backscattering geometry using a Jobin Yvon HR800 micro-Raman spectrometer (λ_{exc} = 325 nm), with a 40× microscope quartz objective.

3. RESULTS & DISCUSSION

Figure 3 shows SEM images for fracture cross-sectional samples of NiO and ZnO grown by PLD on Si(111) substrates under the same conditions (and for the same duration) as the growths on the FTO/glass and bulk ZnO.

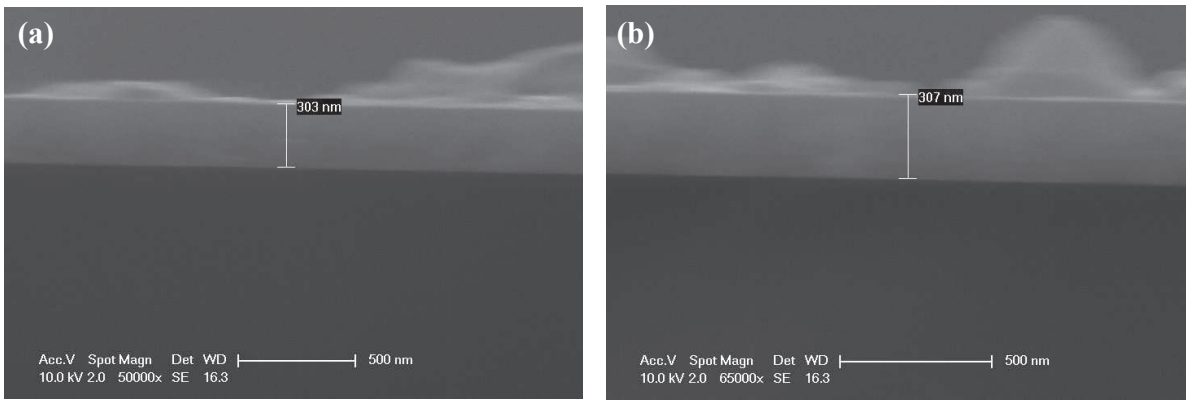

Figure 3. SEM images of fracture cross-sections of (a) NiO and (b) ZnO grown by PLD on Si(111) under the same conditions as those used for the heterojunction growth.

The NiO and ZnO layers show film thicknesses of 303 and 307 nm, respectively.

3.1 NiO grown on bulk hydrothermal ZnO substrates

Figure 4 shows typical SEM images before and after NiO growth on the hydrothermal bulk ZnO substrate.

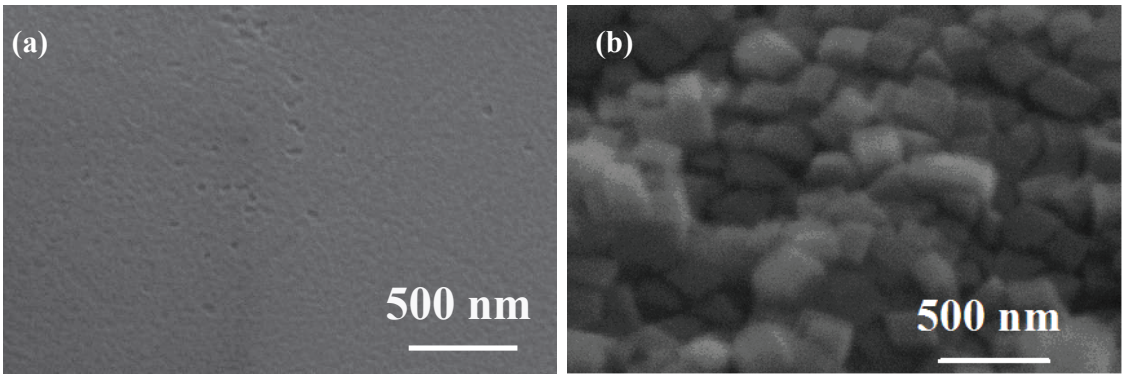

Figure 4. SEM images for (a) the bulk hydrothermal ZnO substrate and (b) the NiO grown by PLD on the bulk hydrothermal ZnO substrate.

The SEM image for the surface of the bulk ZnO substrate reveals a relatively smooth morphology with no evidence of crystallites but which has some striations and pits, which may have their origin in the chemical-mechanical polishing used to prepare the substrate surface. The SEM image for the surface of the PLD NiO grown on the bulk hydrothermal ZnO shows well-defined and randomly-oriented cubic grains which are all about 200-300 nm in diameter.

Figure 5 shows the corresponding XRD 2θ–ω scan for the NiO/bulk ZnO.

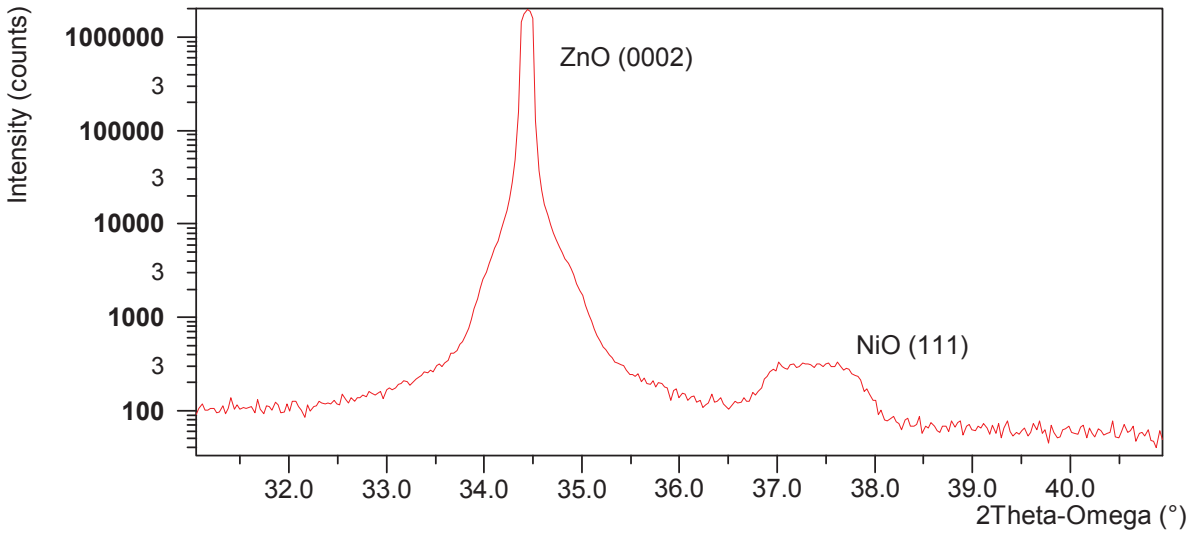

Figure 5. XRD 2θ–ω scan for the NiO grown on bulk ZnO.

The scan shows a strong wurtzite ZnO (0002) peak associated with the bulk substrate and a weaker peak which can be indexed as the (111) reflection of fcc NiO.

Figure 6 shows the schematic of the lateral device architecture and contacting approach employed for electrical transport study of the p-NiO/bulk n-ZnO heterojunction.

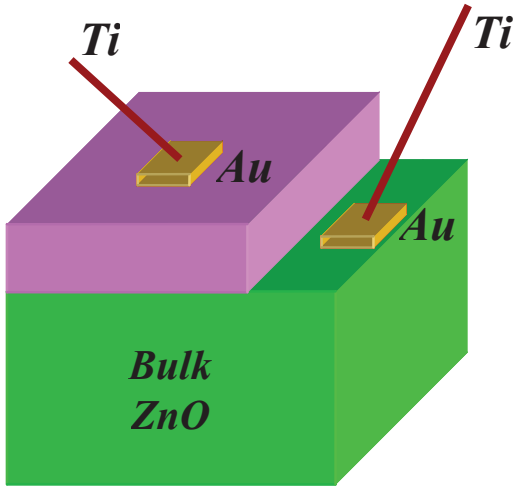

Figure 6. Schematic of the lateral device architecture adopted for the p-NiO/bulk n-ZnO heterojunction.

The NiO mesa was about 6mm x 6mm in size and was realised by employing a shadow mask during the PLD growth of the NiO layers. The contacts were made using the Ti probes of the probe station to apply pressure to gold foil.

Figure 7 shows typical n-n and p-p I/V curves for the electrical contacts.

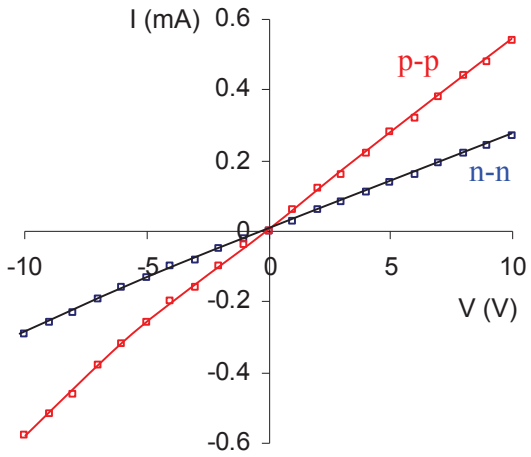

Figure 7 n-n and p-p I/V curves for the p-NiO/n-ZnO heterojunction grown on bulk ZnO.

Good Ohmic response was obtained between -10 and +10V for both the n-n and p-p contacts. The n-n and p-p resistances were ~40kΩ & ~20kΩ, respectively (attempts using indium contacts gave a Schottky response)

Figure 8 shows two typical dark I/V curves for the heterojunction acquired using different n-contact positions on the bulk ZnO substrate.

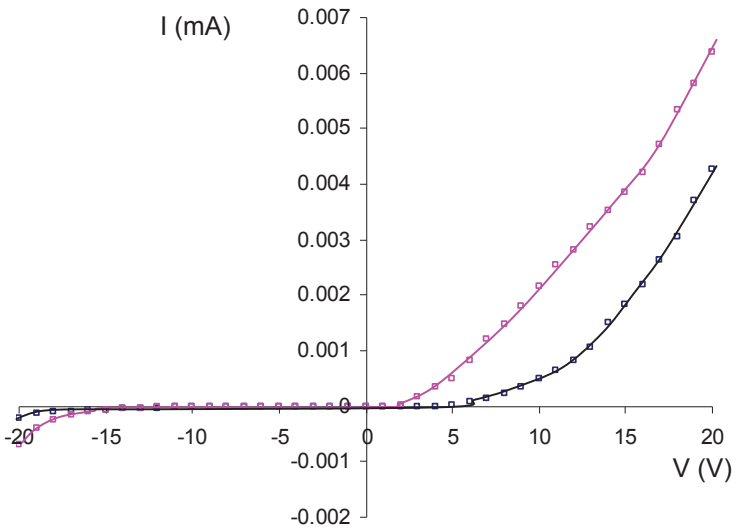

Figure 8 Two typical dark I/V curves for different contacting positions on the p-NiO/bulk n-ZnO heterojunction.

Both the I/V characteristics show clear rectifying behavior as would be expected for a p-n junction. The switch-on voltages (Von) varied between about 2 and 5V, which is in the approximate range that would be expected for the bandgaps of ZnO and NiO. For 10V of reverse bias the leakage current was ~ 10^{-7} A. The forward currents for the different lateral ZnO contact positions were both in the μA range but showed a significant dependence contact position (0.5 vs 2.2 μA at +10V). Four point resistance measurements revealed the bulk ZnO to have an elevated resistivity of > 10^5 Ω.cm. Thus the observed variations of the I/V characteristic with contact position could be related to the relatively low conductivity of the ZnO bulk substrate causing series resistance and current crowding issues.

3.2 NiO/ZnO heterostructure grown on FTO / glass

Figure 9 shows typical SEM images for the FTO, ZnO and NiO surfaces.

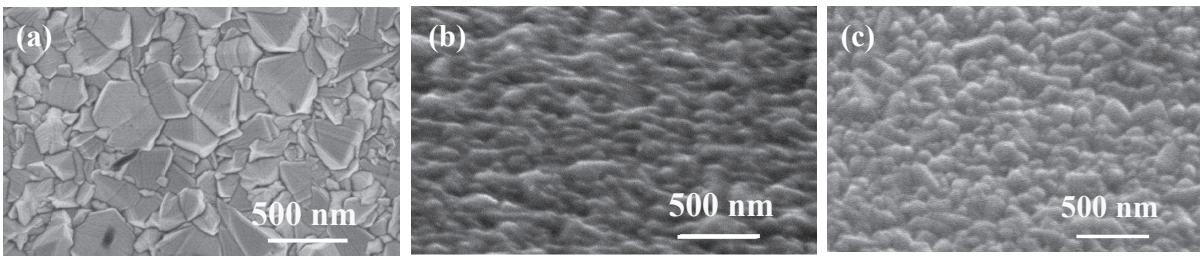

Figure 9. SEM images of the a) FTO/glass b) ZnO/FTO/glass and c) NiO/ZnO/FTO/glass.

The SEM image for the FTO surface reveals a comparatively coarse granular structure exhibiting well-defined crystallites ranging in diameter from ~30 to ~400 nm. The images for the NiO and ZnO surfaces both show a finer granularity with less distinct crystallites.

Figure 10 shows the corresponding XRD 2θ–ω scan for the NiO/ZnO/FTO/glass..

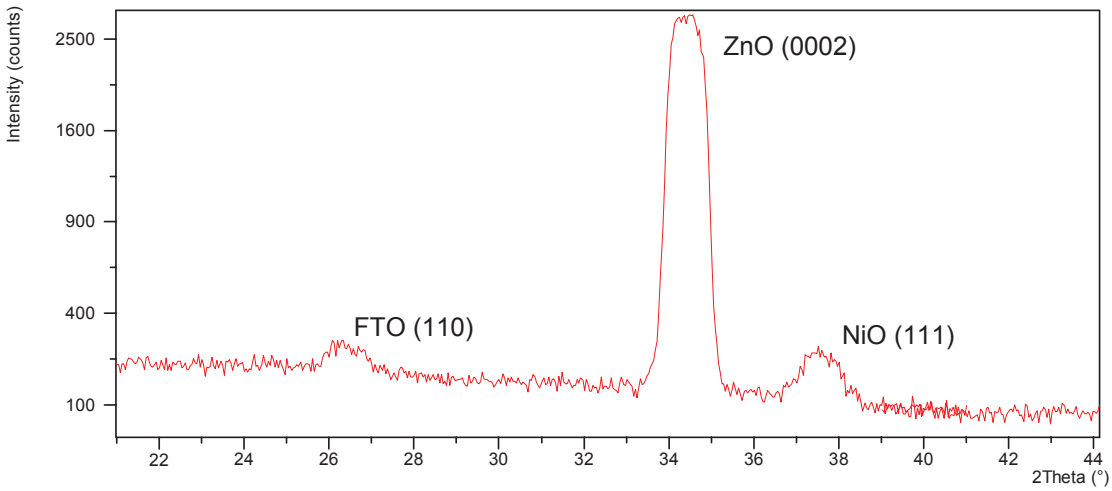

Figure 10. XRD 2θ–ω scan for the NiO/ZnO grown on FTO/Glass.

The scan shows a strong peak which can be indexed as the (0002) peak of wurtzite ZnO straddled by two weaker peaks which can be indexed as the (110) peak of rutile FTO and the (111) peak of fcc NiO. XRD 2θ–ω scans for NiO/FTO/glass (reported previously [12]) did not reveal any peaks that could be indexed to fcc NiO.

Raman spectroscopy was employed to investigate this further. Figure 11 shows Raman spectra for NiO grown directly on FTO/glass.

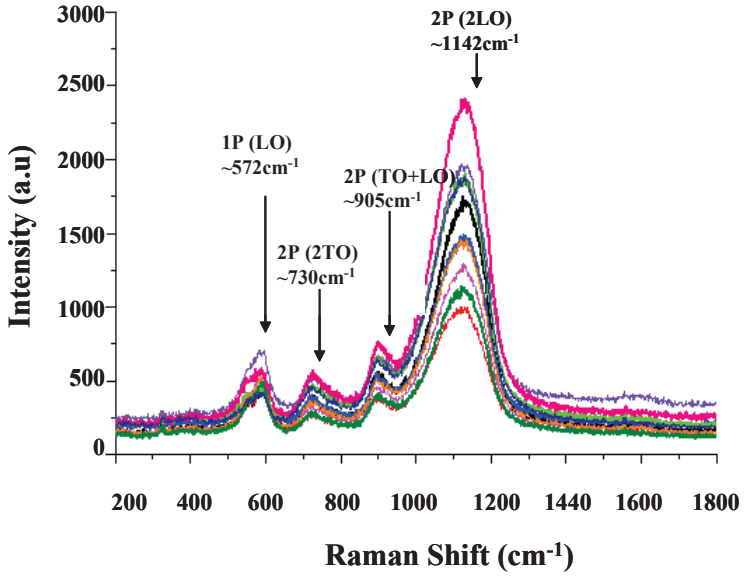

Figure 11. RT Raman spectra for NiO/FTO/glass

The Raman spectra show four main peaks centred at 572, 730, 905 and 1142 cm^{-1}, which agree with values reported in the literature for LO, 2TO and TO+LO for single crystal [22] and nano NiO [23]. Thus, the NiO on FTO was indeed crystallised.

Figure 12 shows the optical transmission curves for FTO/glass, NiO/FTO/glass and NiO/ZnO/FTO/glass.

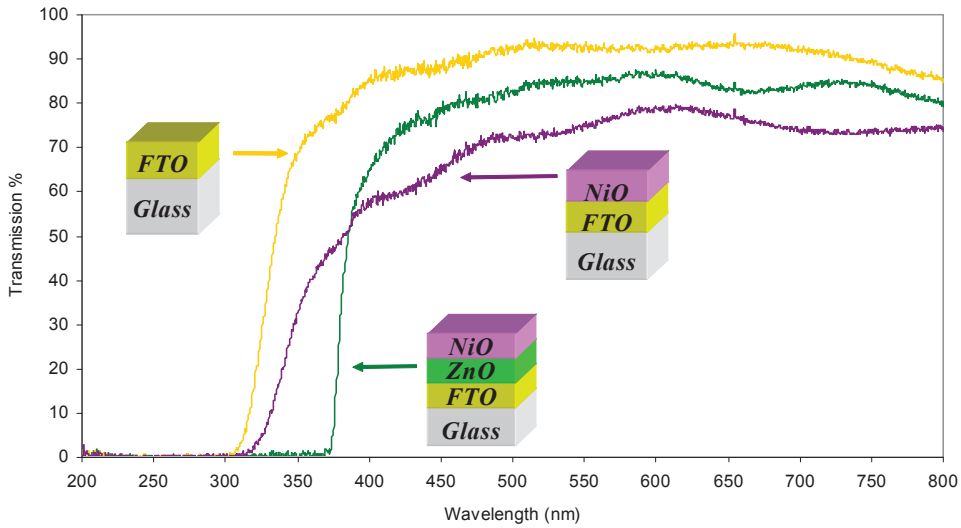

Figure 12. RT optical transmission spectra for FTO/Glass, NiO/FTO/glass and NiO/ZnO/FTO/glass.

The FTO/glass and NiO/ZnO/FTO/glass spectra show relatively abrupt absorption edges compared with that for NiO/FTO. All spectra exhibit extinction in the sub-absorption-edge wavelength range. Bandgap energies were estimated from the intersections with the wavelength axis to be ~ 3.99, ~ 3.70 eV and ~ 3.30 eV for the FTO, NiO and ZnO (respectively). These are consistent with values reported in the literature [9]. The complete stack of NiO/ZnO/FTO/glass showed 80% transparency for almost the whole visible wavelength range which is a relatively high value [9]. Interestingly, the NiO grown directly on FTO/glass showed significantly (~10%) more absorption in the visible wavelength range than the thicker NiO/ZnO/FTO/glass sample. It was postulated, that this poorer transmission and the ill-defined absorption edge could have been due to an increased density of defects introducing color centres in the gap which absorbed in the visible range, as would be expected for the poorer crystal quality implied by the XRD studies.

Figure 13 shows the schematic of the lateral device architecture and contacting approach employed for electrical transport measurements on the p-NiO/n-ZnO heterojunction on FTO/Glass.

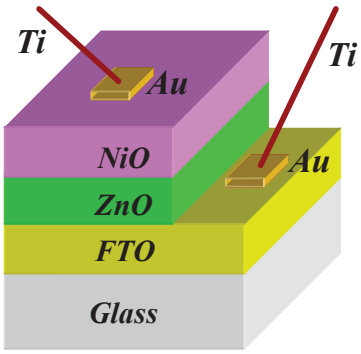

Figure 13. Schematic of the lateral device architecture adopted for the electrical characterisation of the p-NiO/n-ZnO/FTO/glass heterojunction.

The NiO/ZnO mesa was about 6mm x 6mm in size and was realised by employing a shadow mask during the PLD growth of the ZnO and NiO layers. The contacts were made using the Ti probes of the probe station to apply pressure to gold foil.

Figure 14 shows typical n-n and p-p I/V curves for the electrical contacts.

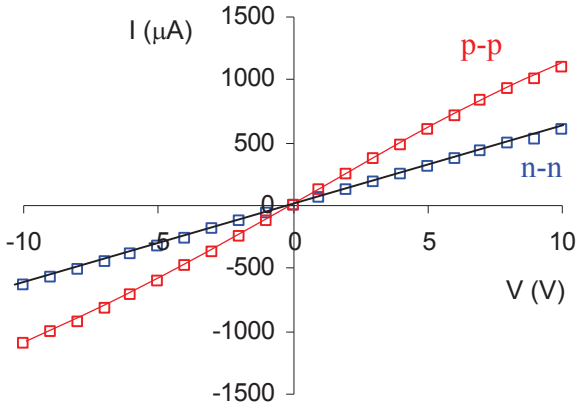

Figure 14 n-n and p-p contact I/V curves for the p-NiO/n-ZnO heterojunction grown on FTO/Glass

Once again, good Ohmic response was obtained between -10 and +10V for both n-n and p-p contacts (attempts using indium contacts gave a Schottky response). The n-n and p-p resistances were ~20 kΩ & ~10 kΩ, respectively. Since the FTO resistivity was in the ~10^{-3} Ω.cm range, each n contact resistance could be estimated as ~10 kΩ.

Figure 15 shows a typical I/V curve for the heterojunction (acquired in the dark).

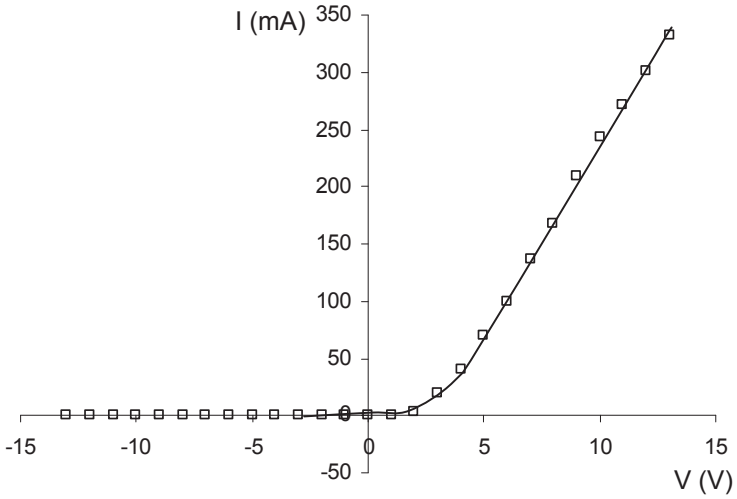

Figure 15 Dark I/V curve for the p-NiO/n-ZnO heterojunctions grown on FTO/glass

Rectifying behavior was observed and forward currents were in the 100s of mA range (243mA at +10V). This is >5 orders of magnitude higher than for the p-NiO/n-ZnO junction formed on the bulk ZnO substrate. There was negligible dependence of the I/V curve on the lateral positioning of the contacts. This is consistent with the much lower resistivity of the FTO back contact improving the current spreading. The Von was ~2V, which is a bit lower than would be expected for the bandgap of the ZnO or NiO. The leakage current was ~ 1.5 x 10^{-5} A for 10V of reverse bias, which is 2 orders of magnitude higher than that observed for the junction on bulk ZnO.

4. CONCLUSIONS

PLD growth was employed to form NiO/ZnO heterostructures on commercial bulk hydrothermal ZnO and FTO/glass substrates. Results of XRD, Raman spectroscopy, optical transmission and SEM studies were consistent with the formation of (0002) oriented wurtzite ZnO and (111) oriented fcc NiO. Introduction of the ZnO layer on FTO appeared to promote improved crystallisation of the NiO overlayer. RT optical transmission studies showed a total transmittance above 80% over the majority of the visible range for the whole NiO/ZnO/FTO/glass stack and allowed bandgap energy estimates of 3.99, ~ 3.70 eV and ~ 3.30 eV for the FTO, NiO and ZnO, respectively. The transmission spectrum for NiO grown directly on FTO showed a less abrupt absorption edge and ~10% less transmission over the visible range than the NiO/ZnO/FTO/glass. It was postulated that this might be due to increased defect density in the NiO/FTO/glass, which is consistent with the poorer crystallinity indicated by the XRD studies.

Lateral device mesas (~6mm x 6mm) were fabricated using a shadow mask during PLD growth. Ti/Au contacting produced Ohmic contacts to the FTO, n-ZnO and p-NiO. The contact resistance for FTO could be estimated at ~10 kΩ. Both kinds of p-n heterojunction showed rectifying I/V characteristics in the dark. The junction on FTO/glass gave forward bias currents (243mA at +10V) that were over 5 orders of magnitude higher for the junction formed on bulk ZnO. Von was observed to vary with contact position for the p-NiO/bulk n-ZnO but not for the p-NiO/n-ZnO/FTO/glass. It was proposed that this might be due to the better conductivity of the FTO reducing current crowding and series resistance issues. At ~ 10^{-7} A for 10V of reverse bias, the leakage current was approximately two orders of magnitude lower on the bulk ZnO substrate than on FTO.

Overall, the lateral p-NiO/n-ZnO heterojunction device grown on FTO/glass was far superior to that formed by growing p-NiO directly on the bulk n-ZnO substrate and gave a combination of electrical performance and visible wavelength transparency that could predispose it for use in various third generation transparent electronics applications.

Acknowledgements

The authors wish to thank the CTU/IEF at the Université de Paris-Sud for access to the SEM and XRD facilities, the French ANR for the funding of the "POSITIF" project and the Portuguese FCT for funding from RECI/FIS-NAN/0183/2012 (FCOMP-01-0124-FEDER-027494) project.

REFERENCES

[1] T. Nozawa, Nikkei Electronics Asia November, (2007) 1024
[2] R. G. Gordon, MRS Bull 25 (2000) 52
[3] D. J. Rogers & F. Hosseini Teherani, Encyclopedia of Materials: Science & Technology, Elsevier, Oxford (2010) 1.
[4] H. Sato, T. Minami, S. Takata, and T. Yamada, Thin Solid Films 236, 27 (1993)
[5] S. Chakrabarty and K. Chatterjee Journal of Physical Sciences, 13 (2009) 245
[6] P. S. Patil & L. D. Kadam (2002) Appl Surf Sci 199:211–221
[7] S. Huffner S (1994) Adv Phys 43:183
[8] L. Ai et al. Applied Surface Science 254 (8), (2008) 2401
[9] V. M. L. Figueireido, PhD. thesis, FCT, Universidade Nova de Lisboa (2012)
[10] F. A. Kröger , J. Phys. Chem. Solids 1968 , 29 , 1889 .
[11] S. Mrowec , Z. Grzesik , J. Phys. Chem. Solids 2004 , 65 , 1651 .
[12] V. E. Sandana et al. Proc. of SPIE Vol. 8987 (2014) 89872P-1
[13] D. J. Rogers et al. Proc. of SPIE Vol. 7605 (2010) 76050K-10
[14] J. C. Fan et al. Progress in Materials Science 58 (2013) 874‑985
[15] Y.Y. Xi et al. Appl. Phys. Lett. 92, (2008) 113505

[16] H. Ohta et al. Appl. Phys. Lett. 83, (2003) 1029
[17] R. Debnath et al. RSC Adv., 2015, 5, 14646
[18] Abbasi et al. Nanoscale Research Letters 2013, 8:320
[19] M. Cavas et al. J Sol-Gel Sci Technol (2012)
[20] N. Münzenrieder et al. Solid-State Electronics 87 (2013) 17–20
[21] D. J. Rogers et al. Appl. Phys. A 88, 49–56 (2007)
[22] R.E. Dietz et al. Phys. Rev.B 42302 (1971).
[23] N. Mironova-Ulmane et al. J. of Phys.: Conf. Series 93, 012039 (2007).